IEEE Access
Multidisciplinary ⋮ Rapid Review ⋮ Open Access Journal

Received 15 November 2024, accepted 30 December 2024, date of publication 2 January 2025, date of current version 8 January 2025.

Digital Object Identifier 10.1109/ACCESS.2024.3525058

RESEARCH ARTICLE

Integrated Detection of Respiration and Heartbeat With Communication Capabilities Using OFDM-LFM-MP Signals

ZHAOSHEN DONG[1], YAN LIU[1,2], AND YUKAI OUYANG[1]
[1]Department of Electrical and Electronic Engineering, The Hong Kong Polytechnic University, Hong Kong
[2]China United Network Communications Company Ltd., Jiangsu Branch, Nanjing 210019, China

Corresponding author: Zhaoshen Dong (zhao-shen.dong@connect.polyu.hk)

ABSTRACT To address the evolving demands of intelligent networks, integrated sensing and communication (ISAC) has emerged as a focal area of research. This encompasses innovative signal design, radar-based and communication hardware integration, and other vital directions. In particular, Linear Frequency Modulated (LFM) signals have shown considerable promise in contactless health monitoring applications. This paper presents an integrated radar system design leveraging Orthogonal Frequency Division Multiplexing (OFDM) LFM signals, emphasizing the dual capabilities of communication and sensing. Compared to traditional radar signals, the proposed design enhances information transmission without sacrificing sensing performance. Initially, we developed an OFDM-LFM-MP signal by utilizing M-sequences with strong auto-correlation properties for coding communication data. Subsequently, we conduct MATLAB simulations to evaluate the sensing efficacy of the OFDM-LFM-MP signal in detecting heartbeats and respiration alongside its communication performance. Theoretical analyses and simulation outcomes demonstrate that the proposed radar-based integration design significantly improves the detection of heartbeat and respiration while effectively transmitting high-rate information at a signal-to-noise ratio (SNR) exceeding 20 *dB*.

INDEX TERMS Contactless health monitoring, high-rate information, ISAC, M-sequences, OFDM-LFM-MP signal, radar-based integration design.

I. INTRODUCTION

With the exponential growth in the number and applications of communication and wireless sensor devices, there is an increasing shortage of spectrum resources, rising costs of hardware, and significant energy consumption. Consequently, the integrated design of sensing and communication signals has garnered substantial attention and is emerging as a critical enabler for the future of 6G networks [1]. The capacity to collect sensory information from the surrounding environment and transfer this information to other devices is essential for future intelligent IoT networks. Potential applications span numerous environments, including smart homes, smart factories, human-computer interactions, and environmental monitoring.

Integrated Sensing and Communication (ISAC) can be defined as a design methodology and corresponding technology that merges sensing and communication functions, thus optimizing wireless spectrum resource utilization, minimizing hardware costs, and reducing energy consumption to achieve integration gains [1], [2]. Since 1990, researchers have explored the feasibility of implementing ISAC in radar systems, notably through joint beamforming techniques. The earliest instance involved Linear Frequency Modulated (LFM) signals with Π/4-DQPSK modulation [3]. Subsequent research has focused on modulating communication information via LFM signals to yield an integrated waveform that excels in both sensing and communication functionalities.

The associate editor coordinating the review of this manuscript and approving it for publication was Xujie Li.

Currently, ISAC-integrated signaling can be categorized into two main frameworks: co-existence design and co-use design. Co-existence designs may exhibit limited information transmission capability, potentially compromising range resolution for sensing applications [4]. Conversely, co-use designs benefit from advancements in digital signal processing and hardware integration, offering a variety of waveform design solutions such as 2PSK-CDMA-LFM signals [5], CPM-LFM signals [6], and PC-LFM signals [7]. However, these may still incur performance losses in either radar sensing or communication capabilities.

OFDM presents a novel approach for developing integrated waveforms [4], [8]. Currently central to 4G and 5G communications, OFDM—paired with LFM signals—is predominantly utilized in radar for wireless sensing. Remarkably, communication and sensing devices have evolved in similar directions over the past decade, leveraging high-frequency bandwidth and large-scale millimeter-wave antenna arrays, thereby enhancing the development of ISAC applications [1], [9], [10]. Consequently, various OFDM-LFM-based integrated signal designs have emerged. For instance, multiple modulation methods have been explored, including OFDM-LFM-QPSK [11], OFDM-LFM-BPSK, OFDM-LFM-MSK, OFDM-LFM-16QAM [12], OFDM-LFM-CPM [13], OFDM-LFM-64QAM [14], etc. While these OFDM-integrated methods demonstrate improved performance, high peak side lobe levels may still adversely affect sensing capabilities [8]. Therefore, further exploration of diverse modulation techniques is warranted to enhance communication capabilities for practical applications.

The demand for health monitoring has significantly increased in recent years, with the assessment of respiration and heart rate emerging as essential components in evaluating overall health status. Measuring heart and respiration rates is critical in detecting conditions such as sleepiness, apnea, cardiac arrest, and other health issues [15], [16], [17]. Traditional monitoring devices, including oximeters and patch-based ECG signal detectors, are predominantly contact-based. This requirement for physical contact limits their convenience for daily use and poses challenges for monitoring newborns or patients with burn injuries [18], [19], [20].

Consequently, there is growing interest in non-contact monitoring solutions [21], such as EverOn^{TM} [22] and sensing radars [16]. Many researchers have explored algorithms for contactless radar detection of vital signs using LFM signals [17], [23], [24]. However, in specific scenarios, such as earthquakes and battlegrounds, the scarcity of spectrum and power resources necessitates the use of OFDM combined with LFM signals, which can facilitate both communication and vital human signal detection while conserving resources—an approach of vital importance for the future.

Nowak et al. [25] introduced a hybrid modulation technique for LFM-MP signals using M-sequences and Intended Modulation on Pulse (IMOP). While this method enhances the communication performance of integrated signals, it does not effectively improve radar sensing capabilities. This paper proposes a novel signal based on the LFM-MP signal, employing phase-coded modulation with the OFDM technique [26], [27]. We call it the (orthogonal frequency division multiplexing—linear frequency modulated -M sequences-phased) **OFDM-LFM-MP** signal. Our integrated signal prioritizes communication transmission efficiency while concurrently enhancing radar sensing performance.

Subsequently, we evaluate the OFDM-LFM-MP signal using MATLAB to assess its ability to monitor breathing and heartbeat. A schematic of the proposed system is illustrated in Fig. 1, where the transmitter simultaneously sends information to the receiver while receiving the reflected OFDM-LFM-MP signal from the human body, which is then processed to extract respiration and heart rates. This way does not need the other controllers and hubs (network equipment), which can reduce dealing time consumption and security concerns for traveling over the network.

The structure of this paper is organized as follows: Section II outlines the inference process for the OFDM-LFM-MP signal model and presents the waveforms for LFM, LFM-MP, OFDM-LFM, and OFDM-LFM-MP signals. Section III evaluates the performance of the OFDM-LFM-MP signal in communication and sensing functions and its complexity analysis, respectively. Section IV simulates a health monitoring system utilizing the OFDM-LFM-MP signal to investigate its application in the health sector. Finally, conclusions are drawn in Section V.

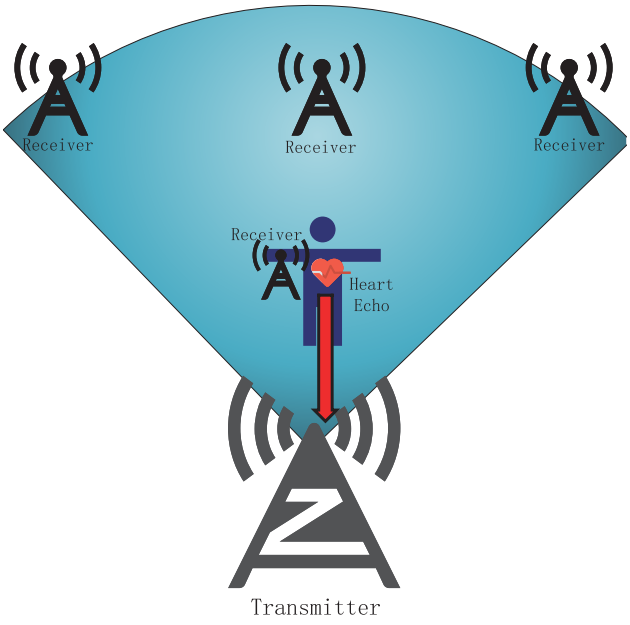

FIGURE 1. A diagram of the OFDM-LFM-MP signal health monitoring system.

II. SIGNAL MODELING

A. LFM SIGNAL MODELING

LFM signals, commonly used in modern radars, have a linear correspondence between time and frequency. We first present the mathematical model expression for the LFM chirp signal [3], [28], as in

$$x_L(t) = A(t)\exp(j2\pi f_0 t + j\mu t^2\pi + j\theta), \quad 0 \le t \le T \quad (1)$$

where $A(t)$ is the amplitude of the LFM chirp signal, f_0 the start frequency, μ the chirp rate, θ a phase constant of the chirp signal, and T the duration of a chirp pulse. The frequency range of the LFM chirp signal is from f_0 to f_c, and f_c is the cut-off frequency that can be given by

$$f_c = f_0 + \mu T\ . \quad (2)$$

B_{LFM} is the chirp bandwidth, which is defined as

$$B_{LFM} = |\mu|T\ . \quad (3)$$

The waveform of the LFM chirp signal in the time domain is shown in Fig. 3(a).

B. LFM-MP SIGNAL MODELING

M-sequence is an excellent method for modulating information into the LFM signal, which can be defined as the binary sequence. Its advantages include long periods, good autocorrelation properties, good inter-correlation properties, good randomness, good immunity to jamming, and good immunity to multipath fading [29], [30]. By using preferably more than one M-sequence, we can increase the number of bits to carry the information. As a consequence, the mathematical expression of the LFM-MP signal [25] is represented by

$$\begin{aligned} x_{LMP}(t) = &\sum_{i=0}^{P-1}\sum_{\mu=0}^{M-1} P_c(t - iT_b - \mu T_c) \\ &\times\ A_c\cos(2\pi f_0 t + \mu t^2\pi + (b_i^1 c_\mu^1 \\ &+ b_i^2 c_{\mu-Q}^2)\theta_I + \theta). \end{aligned} \quad (4)$$

The waveform of the LFM chirp signal in the time domain is shown in Fig. 3(b).

C. OFDM-LFM SIGNAL MODELING

OFDM signaling is a method of frequency multiplexing in which the transmitted signal is transmitted in parallel over several orthogonal subcarriers. OFDM has a lower symbol rate than the single-carrier regime with a defined data rate, but several signals can be transmitted simultaneously. The OFDM modulation technique separates the signals by modulating the data on orthogonal sub-carriers and transmitting the modulated signals. The receiver achieves the separation of each signal by means of the orthogonality between the sub-carrier frequencies.

In this paper, the OFDM signal expression is used as follows

$$x_O(t) = \sum_{h=0}^{N_s-1}\sum_{k=0}^{N_c-1} rect(t - hT_s)\times\exp(j2\pi(f_0 + k\Delta f)t) \quad (5)$$

where N_s is the symbolic number, N_c the number of sub-carriers, $rect(t)$ the rectangular window, T_s the modulating the time width occupied by 1 bit, Δf the sub-carrier frequency interval.

Then, we can get the routine joint OFDM-LFM signal [31] by (5) shown as

$$\begin{aligned} x_{OL}(t) = &\sum_{h=0}^{N_S-1}\sum_{k=0}^{N_c-1} rect(t - hT_s) \\ &\times\exp(j2\pi(f_0 + k\Delta f)t + j\mu t^2\pi + jb_{h,k}\theta_{O-L}) \end{aligned} \quad (6)$$

where $b_{h,k}$ is the hth bipolar bit information modulated on the kth sub-carrier, θ_{O-L} is the phase of the modulation on the sub-carrier. The waveform of the OFDM-LFM signal in the time domain is shown in Fig. 3(c).

D. OFDM-LFM-MP SIGNAL MODELING

From the result of (4) and (6), we can get the new joint signal which is named OFDM-LFM-MP. It's mathematical expression is

$$\begin{aligned} x_{OLMP}(t) = &\sum_{h=0}^{N_s-1}\sum_{k=0}^{N_c-1}\sum_{z=0}^{Z-1} rect(t - hT_s - zT_m) \\ &\times\exp(j2\pi(f_0 + k\Delta f)t + j\mu t^2\pi \\ &+ jb_{h,k}^1\theta_{O-L}M_{1,z} + jb_{h,k}^2\theta_{O-L}M_{2,z}) \end{aligned} \quad (7)$$

where Z is the length of M_1 and M_2 [25], $b_{h,k}^1$ the hth bit in the information stream b^1 modulated on the kth sub-carrier, $b_{h,k}^2$ the hth bit in the information stream b^2 modulated on the kth sub-carrier, $M_{1,z}$ the zth value in the M_1 sequence, $M_{2,z}$

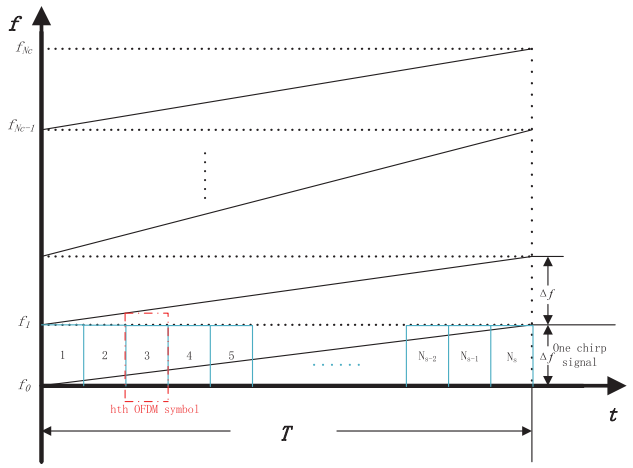

FIGURE 2. Time-frequency diagram of the OFDM-LFM-MP signal.

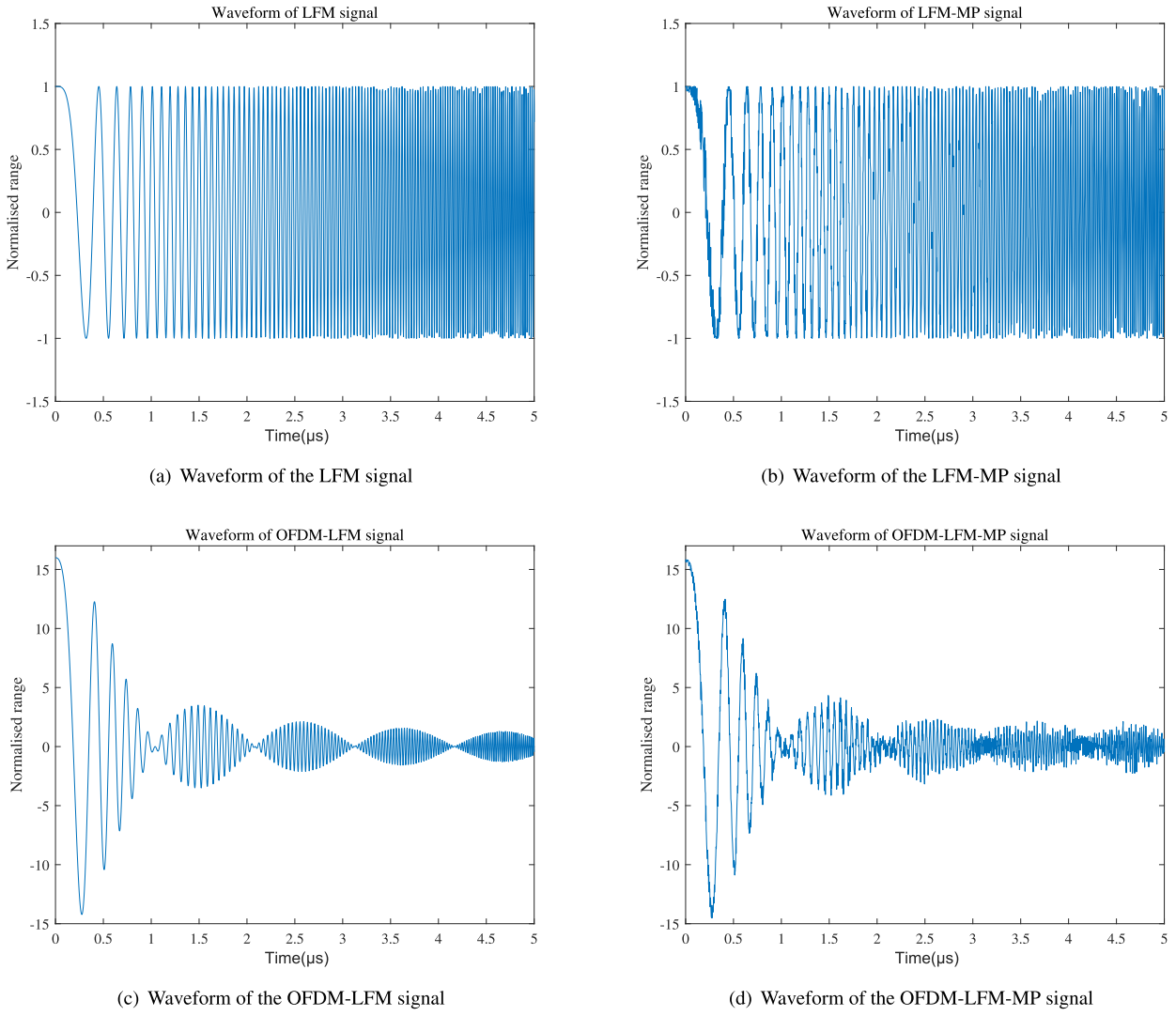

(a) Waveform of the LFM signal

(b) Waveform of the LFM-MP signal

(c) Waveform of the OFDM-LFM signal

(d) Waveform of the OFDM-LFM-MP signal

FIGURE 3. Four kinds of signal waveforms in the time domain.

the zth value in the M_2 sequence, T_m the unit length of time-width occupied by one communication bit. The waveform of the OFDM-LFM-MP signal in the time domain is shown in Fig. 3(d).

The structure of the time-frequency diagram of the OFDM-LFM-MP integrated signal is shown in Fig. 2, which makes it clearer to understand this new signal. OFDM technology increases the bandwidth of the LFM-MP signal that the new bandwidth B_{OLMP} can be expressed as

$$B_{OLMP} = N_C \times B_{LFM}. \tag{8}$$

E. SIGNAL WAVEFORM SIMULATIONS

These four signal waveforms in section II are presented in Fig. 3.

III. OFDM-LFM-MP SIGNAL PERFORMANCE EVALUATION

The radar-communication integrated signal is the signal applied in the radar-communication integrated system that can simultaneously realize radar target detection and communication information transmission. Due to the different functions of radar and communication systems, their signal requirements are also different. When designing a radar-communication integrated signal, it is necessary to take into account the different signal requirements of radar and communication systems. In this section, we evaluate the performance of the newly synthesized OFDM-LFM-MP signals in Matlab in terms of their performance in the communication and sensing domains. The parameters of the evaluations are expressed in the Table 1.

A. COMMUNICATION ANALYSIS

1) COMMUNICATIONS RATE

In this paper, the bit rate of information transmission rate is used as a criterion for judging the communication transmission rate, i.e., the number of bits of information transmitted per unit of time. The communications rate's

mathematical expression is

$$RATE = R_B \log_2^E \quad (bit/s) \tag{9}$$

where E denotes the encoding mechanism (the M-sequence in this paper is a binary system, E=2) and R_B indicates the number of code elements transmitted per unit of time.

In order to provide a sufficient signal-to-noise ratio, we used a 6-order linear shift register to generate the M-sequence. The period of this M-sequence is shown in

$$\begin{aligned} P &= 2^{\mathrm{n}} - 1 \\ &= 2^6 - 1 = 63. \end{aligned} \tag{10}$$

That is, a communication bit occupies a time width of T_b

$$\begin{aligned} T_b &= P * T_s \\ &= 63 \times 2.5 = 157.5(ns). \end{aligned} \tag{11}$$

The time width of the OFDM-LFM-Comm beam is T_p

$$\begin{aligned} T_p &= (N_s - 1) \times T_s \\ &= 8191 \times 2.5 = 20.4775(\mu s) \end{aligned} \tag{12}$$

so that the bits of information can be modulated on each sub-carrier by a pair of M-sequences is B_P

$$\begin{aligned} B_P &= 2 \times (N_s/P) \\ &= 2 \times (8192/63) = 260(bit). \end{aligned} \tag{13}$$

As a result, we can get the communication rate in the following equation by the (9)

$$\begin{aligned} RATE &= N_c \times \frac{1}{T_p/D_c} \times B_P \times \log_2^E \\ &= 243.78(Mbit/s). \end{aligned} \tag{14}$$

TABLE 1. OFDM-LFM-MP simulation parameters.

Parameters (Symbol)	Value (Units)
Chirp time-width (T_p)	20.4775 (μs)
Sampling frequency (F_s)	400 (MHz)
Sampling interval (T_s)	2.5 (ns)
Sampling point (N_s)	8192
M sequence length (P)	63
Number of bits carried by sub-carrier (B_P)	260 (bit)
Number of sub-carriers (N_c)	64
Signal Gain (G_s)	0 (dB)
Original frequency (f_0)	6 (MHz)
Sub-carrier frequency interval (Δf)	6 (MHz)
Radio Frequency(RF) (f_R)	28 (GHz)
Radar scattering cross section product (R_s)	1 (m^2)
Duty cycle (one chirp) (D_c)	30%

Compared with the LFM-MP signal, which only has one sub-carrier with a lower communication rate of 3.81 $Mbit/s$ in the same environment, their relationship is shown as

$$RATE = N_c \times R_{LFM}. \tag{15}$$

From the communications rate analysis, it is clear that as the number of sub-carriers increases, the communication transmission rate increases.

2) BANDWIDTH UTILIZATION

Bandwidth utilization is an indication of the communication efficiency of different communication systems and is defined as the ratio of communication rate to bandwidth. Its mathematical expression is

$$\begin{aligned} B_\mu &= \frac{RATE}{B_T} \times 100\% \\ &= 63.5\% \end{aligned} \tag{16}$$

which shows that the integrated OFDM-LFM-MP signal in this paper has high spectrum utilization.

3) BIT ERROR RATE

The bit error rate(BER) is an essential criterion to measure the communication performance of a signal. The BER(P_e) is defined as the ratio between the number of code elements that are demodulated incorrectly by the communication receiver(P_w) and the total number of transmitted code elements(P_T) and is given by the expression

$$P_e = \frac{P_w}{P_T}. \tag{17}$$

In this part of the evaluation, we use random binary numbers as the transmission sequence. As a result, the example of the reception sequence at a Signal-to-noise ratio(SNR) of 15dB is shown in Fig. 4, where we can observe the bit error in the red circle.

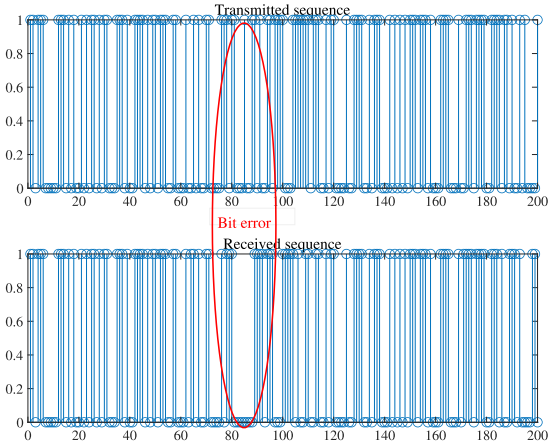

FIGURE 4. Example of the bit error at an SNR of 15*dB*.

However, the trend of BER has an increasing number of sub-carriers. The number of sub-carriers is taken as 64, 128, and 512, and the simulation results are shown in Fig. 5.

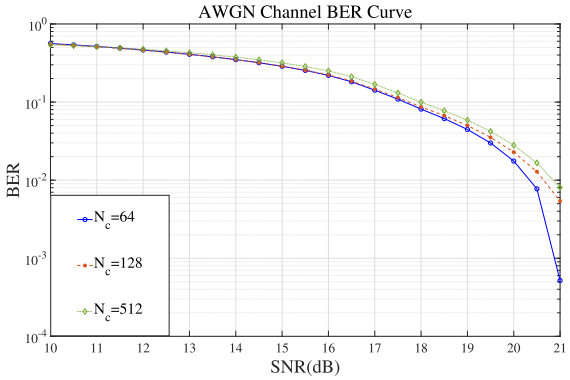

FIGURE 5. The diagram of the BER curve in three kinds of sub-carrier number.

From the BER analysis, under a certain number of carriers, the BER of the communication increases with the increase of the SNR. Under the same SNR condition, the BER of the communication increases with the number of OFDM-LFM-MP sub-carriers, which is consistent with the actual situation. In order to achieve a BER of less than 10^{-2}, the design signal requires an SNR is about $20dB$ higher than that required for OFDM-LFM-MP phase-modulated signals.

The designed OFDM-LFM-MP signals have the form of OFDM signals and retain the advantages of OFDM signals to achieve high-speed communication transmission, high spectrum utilisation and high communication accuracy. In order to make the integrated signal communication performance better, the parameter design should try to make the communication rate higher and the BER lower and for the radar system, its primary purpose is to detect the target, so we also need to explore its sensing ability.

B. SENSING ANALYSIS

1) AMBIGUITY FUNCTION ANALYSIS

The ambiguity function of the radar is one of the crucial references for the design of the sensing signal [32], [33], which of the radar can be used to briefly analyze the signals of the designed transmitter signals and the corresponding filters to analyze the signal in terms of resolution, fuzziness, parameter estimation accuracy, and clutter suppression ability so as to quantitatively obtain the resolution of the radar to detect the target.

The conventional ambiguity function of the sensing signal $x(t)$ has a mutual correlation between the signal and its time-delayed version [34], [35], [36], in which mathematical expression is shown as

$$|\chi_s(\tau, F_d)| = \left| \int_{-\infty}^{\infty} x(t) x^*(t-\tau) \exp(j2\pi F_d t) dt \right| \tag{18}$$

where τ is the relative time delay between the two targets, F_d the relative Doppler frequency-shift, and $x^*(t-\tau)$ is the conjugate of the $x(t)$ time-delayed signal.

We first investigate the nature of the ambiguity function of the LFM signal by (1) and (18), as given in

$$\begin{aligned} &|\chi_{s-LFM}(\tau, F_d)| \\ &= \left| \int_{-\infty}^{\infty} x_L(t) {x_L}^*(t-\tau) \exp(j2\pi F_d t) dt \right| \\ &= \begin{cases} \left| \left(1-\frac{\tau}{T}\right) \frac{\sin(\pi T(F_d+\mu\tau)(1-\frac{\tau}{T}))}{\pi T(F_d+\mu\tau)(1-\frac{\tau}{T})} \right|, |\tau| \le T \\ 0, |\tau| > T \end{cases} . \end{aligned} \tag{19}$$

and the ambiguity function result is shown in Fig. 6(a).

According to the ambiguity function as shown in (19), we can pay more attention to its two properties, which are the Doppler cut at zero range and the Doppler cut at zero delay [34].

Making F_d=0 in (19) gives the Doppler cut at zero range

$$\begin{aligned} |\chi_{s-LFM}(\tau, 0)| = &|\sin c\left[\pi\mu\tau(T-\tau)\right] \\ &\times \left(1-\frac{\tau}{T}\right)|, |\tau| \le T \end{aligned} \tag{20}$$

Making τ=0 in (19) gives the Doppler cut at zero delay

$$|\chi_{s-LFM}(0, F_d)| = |\sin c(\pi T F_d)|, |\tau| \le T \tag{21}$$

where $\sin c(x) = \sin(x)/x$ is the one-dimensional normalised Singh function.

The nature of the ambiguity function of the LFM-MP signal by (4) and (18), as given in

$$\begin{aligned} &|\chi_{s-LMP}(\tau, F_d)| \\ &= \left| \int_{-\infty}^{\infty} x_{LMP}(t) {x_{LMP}}^*(t-\tau) \exp(j2\pi F_d t) dt \right| \end{aligned} \tag{22}$$

because the LMF-MP signal carries modulated random communication information, the exact mathematical formulas are inconvenient to derive. However, since the performance of the radar is not significantly affected by small changes in the addition of short duration discrete phase, its ambiguity function is very similar to that of the LFM signal [25], and the ambiguity function result is shown in Fig. 6(b).

The nature of the ambiguity function of the OFDM-LFM signal by (6) and (18), as given in

$$\begin{aligned} |\chi_{s-OL}(\tau, F_d)| &= \left| \int_{-\infty}^{\infty} x_{OL}(t) {x_{OL}}^*(t-\tau) \exp(j2\pi F_d t) dt \right| \\ &= |\exp(-j2\pi\mu\tau^2) \\ &\quad \times \int_0^{T_s-|\tau|} \sum_{k_1=0}^{Nc-1} \sum_{k_2=0}^{Nc-1} \exp(j2\pi(f_0 + k_2\Delta f)\tau) \\ &\quad \times \exp(j2\pi(k_1-k_2)\Delta f t) \\ &\quad \times \exp(j2\pi(F_d+\mu\tau)t) dt| \\ &= |\chi_{auto}(\tau, F_d) + \chi_{cross}(\tau, F_d)|, |\tau| \le T_s \end{aligned} \tag{23}$$

which $\chi_{auto}(\tau, F_d)$ is the auto-correlation component of each sub-carrier, and $\chi_{cross}(\tau, F_d)$ is the cross-correlation component between the sub-carriers [37], and the ambiguity function result is shown in Fig. 6(c).

Making $k_1{=}k_2$ gives the ambiguity function of auto-correlation

$$\left|\chi_{k_1=k_2}(\tau, F_d)\right| = \sum_{k_1=0}^{N_c-1} \sum_{k_2=0, k_1=k_2}^{N_c-1} \sin c((F_d - \mu\tau) \times (T_s - |\tau|)) \times (1 - \frac{|\tau|}{T_s}), |\tau| \le T_s. \tag{24}$$

Making $k_1 \neq k_2$ gives the ambiguity function of cross-correlation

$$\left|\chi_{k_1\neq k_2}(\tau, F_d)\right| = \sum_{k_1=0}^{N_c-1} \sum_{k_2=0, k_1\neq k_2}^{N_c-1} \sin c((F_d + (k_1 - k_2)\Delta f - \mu\tau) \times (T_s - |\tau|)) \times (1 - \frac{|\tau|}{T_s}), |\tau| \le T_s. \tag{25}$$

Then, we can obtain the Doppler cut at zero range and the Doppler cut at zero delay of OFDM-LFM signal, respectively, as

$$|\chi_{s-OL}(\tau, 0)| = |\chi_{auto}(\tau, 0) + \chi_{cross}(\tau, 0)|, |\tau| \le T_s \tag{26}$$

$$|\chi_{s-OL}(0, F_d)| = |\chi_{auto}(0, F_d) + \chi_{cross}(0, F_d)|, |\tau| \le T_s. \tag{27}$$

The nature of the ambiguity function of the OFDM-LFM-MP signal by (7) and (18), as given in

$$|\chi_{s-OLMP}(\tau, F_d)| = \left| \int_{-\infty}^{\infty} x_{OLMP}(t) x_{OLMP}{}^*(t - \tau) \exp(j2\pi F_d t) dt \right| \tag{28}$$

which is similar to the LMF-MP signal with modulated random communication information, and the sensing performance of the OFDM-LFM-MP signal is also very similar to the OFDM-LFM signal, and its ambiguity function result is shown in Fig. 6(d).

The normalized comparison of four signals in Doppler cut at zero range and Doppler cut at zero delay is shown in Fig. 7. From the range ambiguity image and the velocity ambiguity images in Fig. 7, we can find that the radar detection ability of the LFM signal is similar to the LFM-MP signal, and it of the OFDM-LFM signal(64-carriers) is also similar to the OFDM-LFM-MP signal(64-carriers). However, the ambiguity function images can only give a rough idea of the radar detection performance but cannot evaluate the integrated signal's target resolution quantitatively. The specific analysis needs to describe the radar detection performance of the proposed integrated signal using peak-to-sidelobe ratio (PSLR) and integrated sidelobe ratio (ISLR) [38], [39].

PSLR indicates the radar's ability to detect different targets. The mathematical expression of the PSLR is given as:

$$PSLR = 20 \log \frac{|P_S|}{|p_M|} \tag{29}$$

where P_S is the highest value of the sidelobe peak, and p_M is the highest value of the mainlobe peak.

ISLR measures the energy leaking from the target's mainlobe as a function of the impulse response. The mathematical expression of the ISLR is given as:

$$ISLR = 10 \log \frac{\int_{-\infty}^{-\tau_I} |\chi(\tau, o)|^2 d\tau + \int_{\tau_I}^{+\infty} |\chi(\tau, o)|^2 d\tau}{\int_{-\tau_I}^{\tau_I} |\chi(\tau, 0)|^2 d\tau} \tag{30}$$

where τ_I is the mainlobe boundary value.

Besides, a smaller PSLR result means a smaller value for the peak of the sidelobe. Similarly, the smaller the ISLR result, the more the signal energy is concentrated in the mainlobe. This paper detects the PSLR and ISLR results of several signals, as shown in Table 2. As we know in Fig. 5, the OFDM-LFM-MP signal with 64 sub-carriers has the better BER, so we choose the OFDM-LFM signal and OFDM-LFM-MP signal with the same number of sub-carriers, and we also compare the PSLR and ISLR of OFDM-LFM-MP signals with other numbers of sub-carriers.

It can be seen in Table 2 that the OFDM-LFM signal with 64 sub-carrier has the best range resolution and the second-best velocity resolution, but it is easy to be jammed. The LFM signal has the fourth-best range resolution and the best velocity resolution and has good immunity to interference. With the increasing number of sub-carriers of the OFDM-LFM-MP signal, its PSLR of range and velocity ambiguity function are much higher. In theory, the auto-correlation of the OFDM chirp waveform is the sum of the auto-correlation and inter-correlation of all the sub-carriers, and the sub-carriers in the same sub-band have a high degree of inter-correlation. Therefore, the general waveform with more sub-carriers has a higher PSLR, severely limiting the radar detection performance [40]. Although the OFDM-LFM-MP signal does not consistently exhibit superior performance in the sensing capability evaluation, it demonstrates a more balanced and comprehensive performance than the LFM, OFDM-LFM, and LFM-MP signals. The OFDM-LFM-MP signal with 64 sub-carriers has the second-best distance resolution and the third-best speed resolution, which has good radar detection capability in addition to good communication capability.

2) SIGNAL COHERENCE

In the actual radar signal processing process, to improve the target detection performance, the accumulation of multiple pulses can generally effectively improve the signal-to-noise Ratio(SNR), thus improving the radar's target detection capability [41], [42]. In the OFDM-LFM-MP ISAC signal designed in this paper, the randomly modulated communication information leads to different phase shifts of different

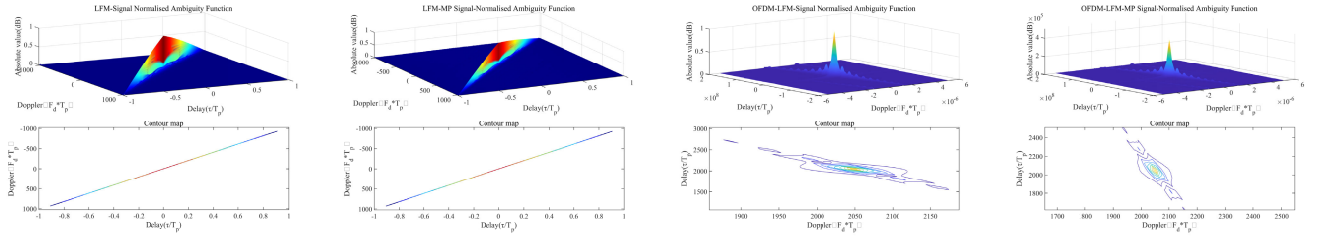

(a) AF of the LFM signal (b) AF of the LFM-MP signal (c) AF of the OFDM-LFM signal (d) AF of the OFDM-LFM-MP signal

FIGURE 6. Ambiguity function chart of four signals.

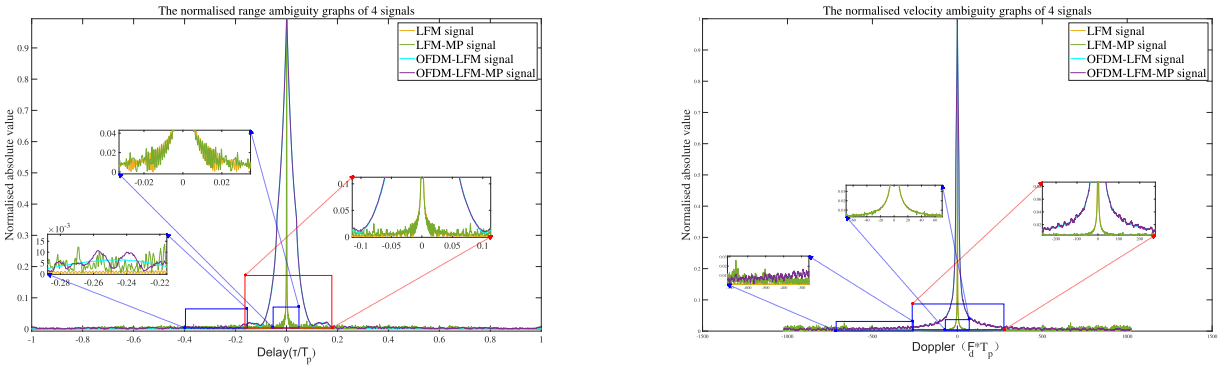

(a) Range ambiguity graph (b) Velocity ambiguity graph

FIGURE 7. Range & Velocity ambiguity function comparison.

TABLE 2. Ambiguity function performance comparison.

Signal	Range ambiguity function		Velocity ambiguity function	
	PSLR(dB)	ISLR(dB)	PSLR(dB)	ISLR(dB)
LFM	-25.5536	-20.3449	-33.5470	-14.1156
LFM-MP	-19.8286	-12.5241	-18.9469	-13.5293
OFDM-LFM(64-carriers)	-40.9288	-3.2765	-25.3518	-4.9854
OFDM-LFM-MP(64-carriers)	-33.8034	-3.2708	-23.3463	-4.9008
OFDM-LFM-MP(128-carriers)	-32.5468	-3.8473	-22.1174	-2.8684
OFDM-LFM-MP(512-carriers)	-6.1405	-3.9143	0	0

inter-pulse signals, which does not allow for strict phase coherent accumulation. To analyse the influence of the communication modulation phase term on the radar phase-coherent processing, we design the vector synthesis process for different phase shift signals, as shown in Fig. 8(a).

In Fig. 8(a), we assume the modulus of the single signal to be 1; signal 1 and signal 2 are the signals of the single signal after phase shift, and the modulus is the same as the original signal; θ_1 and θ_2 denote the absolute magnitude of positive and negative phase shifts. Vector synthesis of signal 1 and signal 2 is performed, and the mathematic modulus of the synthesised signal is calculated using the cosine theorem as $\sqrt{2+2\cos(\theta_1+\theta_2)}$. When θ_1 and θ_2 are both zero or θ_1 and θ_2 are equal, the modulus of the synthesized signal is 2. That is to say, it indicates that the phase shift brought by the communication modulation phase term is the same between different pulses. At this time, the communication modulation will not affect the phase coherence of the signals, and the radar can realize the Phase coherent accumulation. When θ_1 and θ_2 are not equal, the modulus values of the synthesized signal will be smaller than the modulus values of the signal after coherent accumulation. The radar is unable to achieve strict phase-coherent accumulation, which will result in accumulation gain loss.

We evaluate whether the OFDM-LFM-MP signal enables the radar to achieve coherent processing by comparing

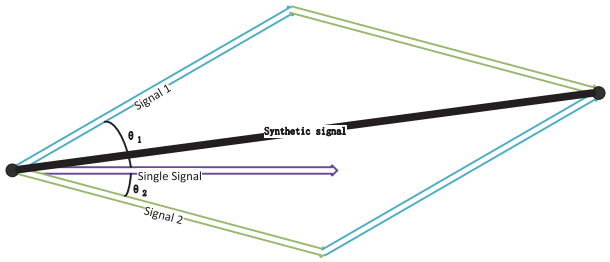

(a) Vector synthesis process for signals with different phase shifts

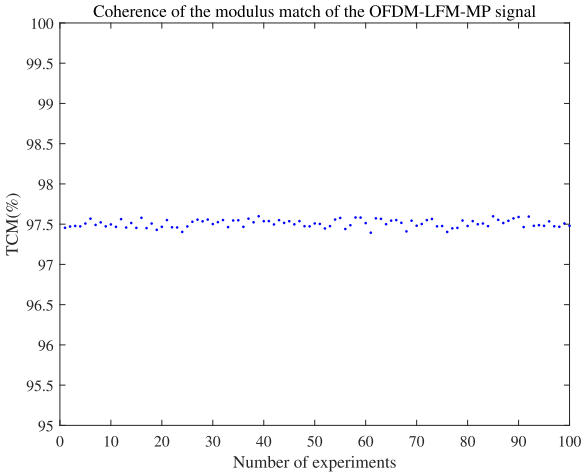

(b) Coherence of the modulus match of the OFDM-LFM-MP signal test

FIGURE 8. **Coherent accumulation test.**

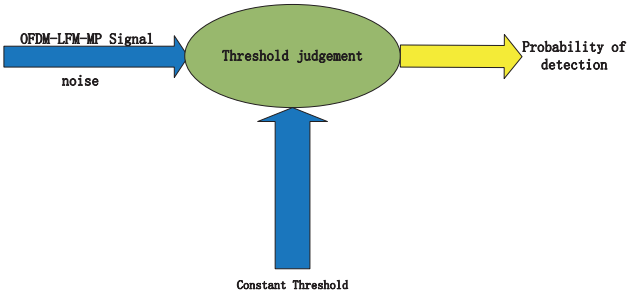

(a) Simplified basic target detection workflows

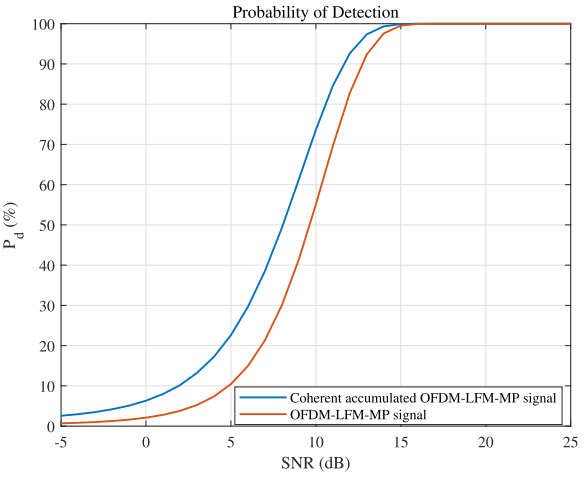

(b) Target detection performance of coherent accumulated OFDM-LFM-MP signal vs. single OFDM-LFM-MP signal

FIGURE 9. **Target detection test.**

the modulus values of 100 output signals (output signals after matched filtering of the coherent accumulated OFDM-LFM-MP signals corresponding to random communication sequences) of the matched filter at the radar receiver, all other things being equal. In this paper, the degree of matching of the modulus values of each output signal is defined as TCM; the smaller the difference in the output signals' modulus values, the larger the TCM and the smaller the accumulated gain loss. The coherence of the modulus match of the OFDM-LFM-MP signal test result is shown in Fig. 8(b); we can find that TCM is stable around 97.5% and the mean value of 100 TCM tests is 97.5080%, which means that the OFDM-LFM-MP signal is not affected too much by communication modulation after coherent accumulation with a little accumulation gain loss.

3) PROBABILITY OF TARGET DETECTION

The primary task of radar is to find a target and to further explore the radar detection performance of OFDM-LFM-MP signals after coherent accumulation; this paper designs a target detection probability experiment, as shown in Fig. 9(a). In this experiment, the false alarm rate P_{far} is 10^{-4} and σ^2 is the total power of noise, then we can get the constant threshold T in (31) [43], [44].

$$T = \sqrt{-\sigma^2 \ln(P_{fap})} \tag{31}$$

This paper uses the target detection probability P_d corresponding to different SNRs under the determined false alarm rate P_{far} as an evaluation criterion for radar target detection performance evaluation standard through a single

OFDM-LFM-MP signal and coherent accumulated OFDM-LFM-MP signals. The number of coherent accumulating is 100, and the Monte Carlo count is 1000. The result is shown in Fig. 9(b), where we can find that the coherent accumulated OFDM-LFM-MP signal has a higher P_d than the single OFDM-LFM-MP signal at the same SNR, which means that the OFDM-LFM-MP signal can approximate coherent accumulation and the random modulated communication do not affect the sensing ability seriously.

C. COMPLEXITY ANALYSIS

In exploring the computational intricacies of M-sequences, phase-modulated information, and OFDM modulation, a layer of heightened complexity emerges. Table 3 prominently dissects the computational complexity [45] of LFM, LFM-MP, OFDM-LFM, and OFDM-LFM-MP signals. The analysis accentuates the substantial influence of synthesizing M-sequences, modulating data with phase information, and adjusting the number of sub-carriers on overall complexity metrics. While orchestrating enhanced communication and sensing capabilities within the amalgamated OFDM-LFM-MP signal, its computational demands outpace those of the other three signal variants. Despite this, these operations predominantly entail low-level processes, leading to negligible impacts on time and space complexity.

IV. OFDM-LFM-MP SIGNAL SIMULATED IN HEALTH MONITORING

After analyzing the performance of OFDM-LFM-MP signals, we started to simulate its sensing application and information transmission function in the health field in MATLAB.

A. MONITORING HEALTH SYSTEM PRINCIPLES AND DESIGN

From Section II and Table 1, we can obtain this system's basic parameters, and then We load the OFDM-LFM-MP signal onto the $30GHz$ carrier. We also know that the frequency range of normal human respiration is 0.1-0.5Hz, the mico-movement of the chest by respiration is 1-12mm, the frequency range of normal human heartbeat is 1-2Hz, and the mico-movement of the chest by heartbeat is 0.1-0.5mm [46]; so we assume that a respiratory motion with a displacement of $5mm$ and a frequency of $0.25Hz$ and a heartbeat motion with a displacement of $0.3mm$ and a frequency of $1.5Hz$ occur in the chest at d_0=$1.2m$ and that radar detects this mixed motion $S(t)$.

A realistic radar component would mix and filter the transmitted and received signals to produce a new signal at a new frequency. Fig. 10 shows the TX and RX OFDM-LFM-MP pulse as a function of time for a single detected object. Note that the RX OFDM-LFM-MP signal is a delayed version of the TX OFDM-LFM-MP pulse, where the delay τ is expressed in (32), and the IF signal is a single-frequency signal with a constant frequency S_τ.

$$\tau = \frac{2dis}{c} \tag{32}$$

where dis is the distance between the radar and the human's chest.

The fact that the phase of the IF signal is susceptible to small movements is the basis for respiratory and heartbeat detection. A micro-movement of the human chest moves Δdis causes the round-trip delay $\Delta\tau$ to change it, and then the phase of the IF signal also changes $\Delta\varphi$ [46]:

$$\Delta\varphi = 2\pi f_c \Delta\tau = \frac{4\pi\,\Delta dis}{\lambda} \tag{33}$$

$$\Delta dis = \frac{\lambda\Delta\varphi}{4\pi} \tag{34}$$

where f_c is the carrier frequency and λ is the wavelength. In this simulation, the reflected signal $RS(t)$ will carry phase-modulated heartbeat and respiration information; we use $\Delta\varphi$ of the phase difference to detect the heart and respiratory frequency in $RS(t)$. Received OFDM-LFM-MP IF signal $RS_{IF}(t)$ after a down-conversion of frequency from $RS(t)$ is expressed as:

$$RS_{IF}(t) = \cos(2\pi S_\tau t + \theta + \frac{4\pi S(t)}{\lambda} + \Delta\Phi(t)) \tag{35}$$

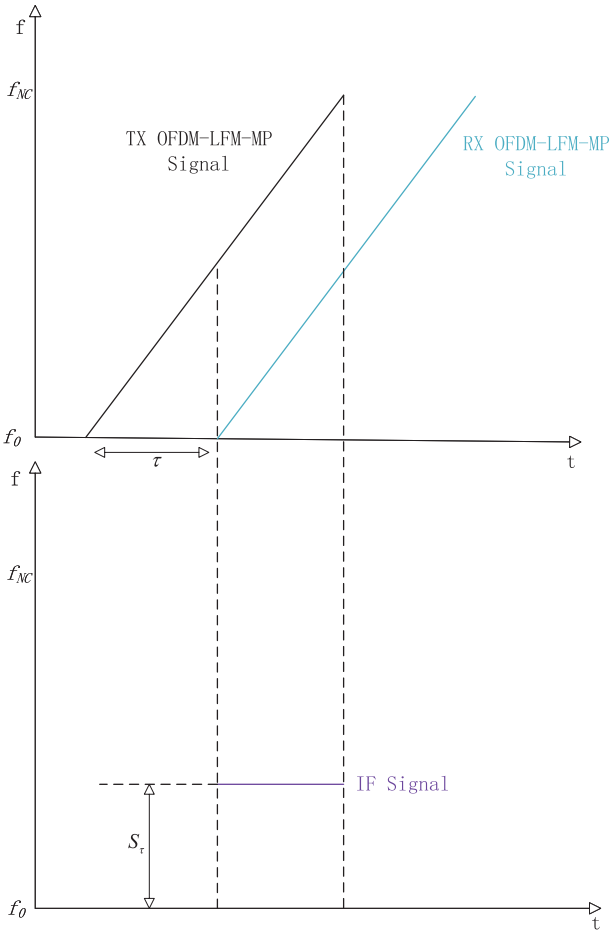

FIGURE 10. IF Signal Frequency Constant.

TABLE 3. Complexity analysis of four signals.

Signals	Time Complexity	Space Complexity	Interpolation
LFM Signal	$O(N_s)$	$O(N_s)$	No
LFM-MP Signal	$O_1(N_s)+O_2(P*n)+O_3(B_p)$	$O_1(N_s)+O_2(P)+O_3(B_p)$	No
OFDM-LFM Signal	$O(N_s*M)$	$O(N_s*M)$	Yes
OFDM-LFM-MP Signal	$O_1(N_s*M)+O_2(P*n)+O_3(B_p*M)$	$O_1(N_s*M)+O_2(P)+O_3(B_p*M)$	Yes

[1] Notes: N_s represents the sampling rates, P represents the period of M-sequence, n represents the number of shift register's order, B_p represents the bits of a pair of M-sequences and M represents the number of sub-carriers.
[2] Notes: O_1 represents the complexity of processing basic signal, O_2 represents the complexity of compiling M-sequence and O_3 represents the complexity of information modulation process.

where θ is the phase shift of mixers and antennas, and $\Delta\Phi(t)$ is the phase noise. Then, we can obtain the received phase $\Delta\phi_{received}$ of the $RS_{IF}(t)$, which compares with the transmitted phase $\Delta\phi_{transmitted}$ of the modulated OFDM-LFM-MP signal to get the phase difference $\Delta\phi$:

$$\Delta\phi = \Delta\phi_{received} - \Delta\phi_{transmitted}. \tag{36}$$

Finally, we utilize (34) and the bandpass filter to handle the phase change $\Delta\varphi$ of $\Delta\phi$ to get the heart and respiratory frequency.

B. MONITORING HEALTH SYSTEM SIMULATION RESULT

This section gives the results of applying the OFDM-LFM-MP signal in this simulation monitoring health system to detect human health information and transmit communication information. Noise signals are incorporated to evaluate and simulate the efficacy of OFDM-LFM-MP signals in the presence of real-world disturbances like body movements, postural changes, and personnel shifts. The SNR quantifies the relationship between the strength of the noise signal and that of the test signal.

Fig. 11 shows the sensing correctness rate of heartbeat and respiration and the random communication information's BER. The set heartbeat frequency and respiratory frequency in this experiment will not change. For sensing ability, we can find that the correctness rate of respiration is stable and higher with the increasing SNR around 99.75% because of the strong breathing amplitude that is easier to detect. The weak heartbeat signals are more difficult to detect until the SNR is greater than 15 when the heartbeat correctness rate stabilized at 91.33%. Regarding communication ability, the BER decreases from an SNR of 13. At an SNR of 20, the BER is already as low as about 10^3, which can be accepted and corrected by the communication system. In this experiment, when the SNR is more than 20dB, the OFDM-LFM-MP signal performs well for monitoring human health information and realizing communication functions simultaneously.

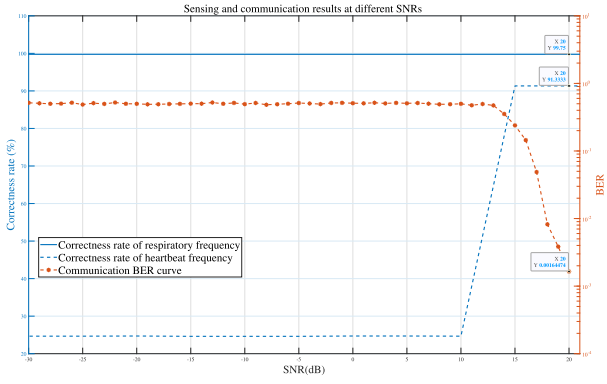

FIGURE 11. Sensing and communication results at different SNRs.

V. CONCLUSION

Integrated sensing and communication (ISAC) represents a significant trend in the evolution of 6G technology, forming the core of future wireless systems. ISAC offers advantages such as low hardware costs, reduced power consumption, and high efficiency in wireless resource utilization, which are critical for advancements in human health monitoring. This paper presents a novel radar communication system, the OFDM-LFM-MP, developed through phase modulation of the OFDM-LFM beam using a spread spectrum M-sequence. Performance analysis demonstrates the advantages that the proposed OFDM-LFM-MP signal significantly enhances data transmission rates within communication systems while accurately allowing radar systems to have target and velocity resolutions without performance degradation. While the computational complexity of the integrated OFDM-LFM-MP signal slightly surpasses that of LFM, LFM-MP, and OFDM-LFM signals, it offers a crucial advantage by enabling the dual functionality of communication and sensing within a single signal. This integration occurs without significant increases in time and space requirements, providing considerable flexibility for specific scenarios. For further research, we focus on designing a comprehensive health monitoring system utilizing the OFDM-LFM-MP signal for simultaneous health information detection and data transmission. The monitoring outcomes illustrate that when the SNR of the simulated environment exceeds 20 dB, the OFDM-LFM-MP signal exhibits robust sensing and communication functionalities performance.

ACKNOWLEDGMENT

(Yan Liu and Yukai Ouyang contributed equally to this work.)

REFERENCES

[1] F. Liu, Y. Cui, C. Masouros, J. Xu, T. X. Han, Y. C. Eldar, and S. Buzzi, "Integrated sensing and communications: Toward dual-functional wireless networks for 6G and beyond," *IEEE J. Sel. Areas Commun.*, vol. 40, no. 6, pp. 1728–1767, Jun. 2022.

[2] S. Lu, F. Liu, Y. Li, K. Zhang, H. Huang, J. Zou, X. Li, Y. Dong, F. Dong, J. Zhu, Y. Xiong, W. Yuan, Y. Cui, and L. Hanzo, "Integrated sensing and communications: Recent advances and ten open challenges," *IEEE Internet Things J.*, vol. 11, no. 11, pp. 19094–19120, Jun. 2024.

[3] M. Roberton and E. R. Brown, "Integrated radar and communications based on chirped spread-spectrum techniques," in *IEEE MTT-S Int. Microw. Symp. Dig.*, vol. 1, Jul. 2003, pp. 611–614.

[4] M. Jiang, G. Liao, Z. Yang, Y. Liu, and Y. Chen, "Integrated radar and communication waveform design based on a shared array," *Signal Process.*, vol. 182, May 2021, Art. no. 107956.

[5] Z. Zhao and D. Jiang, "A novel integrated radar and communication waveform based on LFM signal," in *Proc. IEEE 5th Int. Conf. Electron. Inf. Emergency Commun.*, May 2015, pp. 219–223.

[6] P. M. McCormick, C. Sahin, S. D. Blunt, and J. G. Metcalf, "FMCW implementation of phase-attached radar-communications (PARC)," in *Proc. IEEE Radar Conf. (RadarConf)*, Apr. 2019, pp. 1–6.

[7] F. Uysal, "Phase-coded FMCW automotive radar: System design and interference mitigation," *IEEE Trans. Veh. Technol.*, vol. 69, no. 1, pp. 270–281, Jan. 2020.

[8] D. Dash, A. Jayaprakash, J. Valarmathi, and G. R. Reddy, "Generalized OFDM-LFM waveform design and analysis for multistatic airborne radar," in *Proc. IEEE Power, Commun. Inf. Technol. Conf. (PCITC)*, Oct. 2015, pp. 924–929.

[9] A. Liu, Z. Huang, M. Li, Y. Wan, W. Li, T. X. Han, C. Liu, R. Du, D. K. P. Tan, J. Lu, Y. Shen, F. Colone, and K. Chetty, "A survey on fundamental limits of integrated sensing and communication," *IEEE Commun. Surveys Tuts.*, vol. 24, no. 2, pp. 994–1034, 2nd Quart., 2022.

[10] J. Wang, P. Wang, F. Luo, and W. Wu, "Waveform design and DoA-DoD estimation of OFDM-LFM signal based on SDFnT for MIMO radar," *IEEE Access*, vol. 11, pp. 1348–1358, 2023.

[11] S. Luo, C. Li, L. Wang, and S. Ji, "Research on waveform design of multi-carrier phase coded and frequency modulation signal," in *Proc. CIE Int. Conf. Radar*, Dec. 2021, pp. 1858–1861.

[12] C. Liu, Z. Wang, H. Jiang, and C. Ji, "Communicational radar detection waveform design based on OFDM-LFM," in *Proc. Cross Strait Radio Sci. Wireless Technol. Conf. (CSRSWTC)*, Dec. 2022, pp. 1–5.

[13] G. Wang, Y. Kang, J. Wang, H. Wang, and Z. Zhang, "Research on integrated signal of ofdm-cpm-lfm radar communication," *Microelectron. Comput.*, vol. 40, no. 8, pp. 80–84, 2023.

[14] Q. Ma, J. Lu, and Y. Maoxiang, "Integrated waveform design for 64QAM-LFM radar communication," in *Proc. IEEE 5th Adv. Inf. Technol., Electron. Autom. Control Conf. (IAEAC)*, vol. 5, Mar. 2021, pp. 1615–1625.

[15] K. Nagai and M. Kim, "Contactless simultaneous measurement method for breathing and heartbeat rates using millimeter-waves," in *Proc. 14th Int. Symp. Med. Inf. Commun. Technol. (ISMICT)*, May 2020, pp. 1–4.

[16] J. Chen, D. Zhang, Z. Wu, F. Zhou, Q. Sun, and Y. Chen, "Contactless electrocardiogram monitoring with millimeter wave radar," *IEEE Trans. Mobile Comput.*, vol. 23, no. 1, pp. 270–285, Jan. 2024.

[17] M. Alizadeh, G. Shaker, J. C. M. D. Almeida, P. P. Morita, and S. Safavi-Naeini, "Remote monitoring of human vital signs using mm-wave FMCW radar," *IEEE Access*, vol. 7, pp. 54958–54968, 2019.

[18] T. S. Sollu, M. Bachtiar, and A. G. Sooai, "Patients' heart monitoring system based on wireless sensor network," *IOP Conf. Ser., Mater. Sci. Eng.*, vol. 336, no. 1, 2018, Art. no. 012009.

[19] I.-S. Lee and J.-R. Yang, "Signal preprocessing for heartbeat detection using continuous-wave Doppler radar," *IEEE Microw. Wireless Technol. Lett.*, vol. 33, no. 4, pp. 479–482, Apr. 2023.

[20] D. Obeid, S. Sadek, G. Zaharia, and G. El Zein, "Touch-less heartbeat detection and measurement-based cardiopulmonary modeling," in *Proc. Annu. Int. Conf. IEEE Eng. Med. Biol.*, Aug. 2010, pp. 658–661.

[21] J. A. Walsh, E. J. Topol, and S. R. Steinhubl, "Novel wireless devices for cardiac monitoring," *Circulation*, vol. 130, no. 7, pp. 573–581, Aug. 2014.

[22] J. Ben-Ari, E. Zimlichman, N. Adi, and P. Sorkine, "Contactless respiratory and heart rate monitoring: Validation of an innovative tool," *J. Med. Eng. Technol.*, vol. 34, nos. 7–8, pp. 393–398, Oct. 2010.

[23] S. Wang, A. Pohl, T. Jaeschke, M. Czaplik, M. Köny, S. Leonhardt, and N. Pohl, "A novel ultra-wideband 80 GHz FMCW radar system for contactless monitoring of vital signs," in *Proc. 37th Annu. Int. Conf. IEEE Eng. Med. Biol. Soc. (EMBC)*, Aug. 2015, pp. 4978–4981.

[24] F. Wang, X. Zeng, C. Wu, B. Wang, and K. J. R. Liu, "MmHRV: Contactless heart rate variability monitoring using millimeter-wave radio," *IEEE Internet Things J.*, vol. 8, no. 22, pp. 16623–16636, Nov. 2021.

[25] M. A. Nowak, Z. Zhang, L. LoMonte, M. C. Wicks, and Z. Wu, "Mixed-modulated linear frequency modulated radar-communications," *IET Radar, Sonar Navigat.*, vol. 11, no. 2, pp. 313–320, Aug. 2016.

[26] X. Tian, T. Zhang, Q. Zhang, and Z. Song, "Waveform design and processing in OFDM based radar-communication integrated systems," in *Proc. IEEE/CIC Int. Conf. Commun. China (ICCC)*, Oct. 2017, pp. 1–6.

[27] X. Tian and Z. Song, "On radar and communication integrated system using OFDM signal," in *Proc. IEEE Radar Conf. (RadarConf)*, May 2017, pp. 318–323.

[28] L. Qi, "Detection and parameter estimation of multicomponent LFM signal based on the fractional Fourier transform," *Sci. China Ser. F, Inf. Sci.*, vol. 47, no. 2, pp. 184–196, 2004.

[29] G. T. Burač as and G. M. Boynton, "Efficient design of event-related fMRI experiments using M-sequences," *NeuroImage*, vol. 16, no. 3, pp. 801–813, Jul. 2002.

[30] S. Linusson, "The number of M-sequences and f-vectors," *Combinatorica*, vol. 19, no. 2, pp. 255–266, Feb. 1999.

[31] X. Mao, B. Cai, M. Xia, and L. Yang, "Research on optimization design method of MIMO radar waveform based on frequency-orthogonal LFM," *IEEE Access*, vol. 12, pp. 160835–160845, 2024.

[32] S. Stein, "Algorithms for ambiguity function processing," *IEEE Trans. Acoust., Speech, Signal Process.*, vol. ASSP-29, no. 3, pp. 588–599, Jun. 1981.

[33] A. Aubry, A. De Maio, B. Jiang, and S. Zhang, "Ambiguity function shaping for cognitive radar via complex quartic optimization," *IEEE Trans. Signal Process.*, vol. 61, no. 22, pp. 5603–5619, Nov. 2013.

[34] R. F. Tigrek, W. J. A. de Heij, and P. van Genderen, "Relation between the peak to average power ratio and Doppler sidelobes of the multi-carrier radar signal," in *Proc. Int. Radar Conf. 'Surveillance Safer World' (RADAR)*, Oct. 2009, pp. 1–6.

[35] G. San Antonio, D. R. Fuhrmann, and F. C. Robey, "MIMO radar ambiguity functions," *IEEE J. Sel. Topics Signal Process.*, vol. 1, no. 1, pp. 167–177, Jun. 2007.

[36] R. Gui, B. Huang, W.-Q. Wang, and Y. Sun, "Generalized ambiguity function for FDA radar joint range, angle and Doppler resolution evaluation," *IEEE Geosci. Remote Sens. Lett.*, vol. 19, pp. 1–5, 2022.

[37] J. Wang, B. Zhang, and P. Lei, "Ambiguity function analysis for OFDM radar signals," in *Proc. CIE Int. Conf. Radar (RADAR)*, Oct. 2016, pp. 1–5.

[38] B. Benmeziane, J.-Y. Baudais, S. Méric, and K. Cinglant, "Comparison of ZF and MF filters through PSLR and ISLR assessment in automotive OFDM radar," in *Proc. 18th Eur. Radar Conf. (EuRAD)*, Apr. 2022, pp. 193–196.

[39] K. Farnane, K. Minaoui, A. Rouijel, and D. Aboutajdine, "Analysis of the ambiguity function for phase-coded waveforms," in *Proc. IEEE/ACS 12th Int. Conf. Comput. Syst. Appl. (AICCSA)*, Nov. 2015, pp. 1–4.

[40] M. Ding, Y. Li, P. Huang, M. Xing, and J. Wei, "An OFDM chirp waveform design method based on multiple groups of subchirp durations optimization for clutter suppression," *IEEE Trans. Geosci. Remote Sens.*, vol. 60, 2022, Art. no. 5120214.

[41] X. Zhang, L. Zuo, D. Yang, and J. Guo, "Coherent-like integration for PD radar target detection based on short-time Fourier transform," *IET Radar, Sonar Navigat.*, vol. 14, no. 1, pp. 156–166, Oct. 2019.

[42] J. Zheng, T. Yang, H. Liu, T. Su, and L. Wan, "Accurate detection and localization of unmanned aerial vehicle swarms-enabled mobile edge computing system," *IEEE Trans. Ind. Informat.*, vol. 17, no. 7, pp. 5059–5067, Jul. 2021.

[43] H. Rohling, "Radar CFAR thresholding in clutter and multiple target situations," *IEEE Trans. Aerosp. Electron. Syst.*, vol. AES-19, no. 4, pp. 608–621, Jul. 1983.

[44] M. A. Richards, J. Scheer, W. A. Holm, and W. L. Melvin, *Principles of Modern Radar: Basic Principles*. Raleigh, NC, USA: SciTech, 2010.
[45] S. Firdaus and M. A. Uddin, "A survey on clustering algorithms and complexity analysis," *Int. J. Comput. Sci. Issues (IJCSI)*, vol. 12, no. 2, pp. 68–79, Jan. 2015.
[46] Texas Instruments. (2024). *TI mmWave Labs-Driver Vital Signs-developer's Guide*. Accessed: 27th Jun. 2024. [Online]. Available: https://dev.ti.com/tirex/explore/node?node=A__ADZIzSoqYpsJx3iqoalh2A__com.ti.mmwave_automotive_toolbox__AocYeEd__LATEST

ZHAOSHEN DONG received the B.Eng. degree from the Information Science and Engineering College, Huaqiao University, Fujian, China, in 2019, and the M.Sc. degree from the Department of Electrical and Electronic Engineering, The Hong Kong Polytechnic University, Hong Kong, in 2024. His research interests include integrated sensing and communication, biomedical signal processing, communication systems, mm-wave radar monitoring of humans, and radar echo signal analysis.

YAN LIU received the Bachelor of Engineering degree in telecommunication engineering from Tiangong University, China, in 2022, and the Master of Science degree in electronic and information engineering from the Department of Electrical and Electronic Engineering, The Hong Kong Polytechnic University, in 2024. His research interests include integrated sensing and communication, wireless data networks, and wireless power transmission.

YUKAI OUYANG received the B.Eng. degree from the College of Electronic Engineering and the College of Artificial Intelligence, South China Agricultural University, Guangzhou, China, in 2020, and the M.Sc. degree from the Department of Electrical and Electronic Engineering, The Hong Kong Polytechnic University, Hong Kong, in 2024. His research interests include integrated sensing and communication, biomedical signal processing, artificial intelligence, and financial technology.